ORIGINAL PAPER

Multi-functional coating of cellulose nanocrystals for flexible packaging applications

Fei Li · Paolo Biagioni · Monica Bollani · Andrea Maccagnan · Luciano Piergiovanni

Abstract In this paper, we systematically address the performance of cellulose nanocrystals (CNs) coated flexible food packaging films. Firstly, the morphology of CNs from cotton linters and homogeneity of its coating on different substrates were characterized by transmission electronic microscopy and atomic force microscopy. Then, the 1.5 μm thick CNs coating on polyethylene terephthalate (PET), oriented polypropylene, oriented polyamide (OPA), and cellophane films were characterized for their mechanical, optical, anti-fog, and barrier properties. CNs coating reduces the coefficient of friction while maintaining high transparency (~90 %) and low haze (3–4 %) values, and shows excellent anti-fog properties and remarkable oxygen barrier (oxygen permeability coefficient of CNs coating, P'O$_2$, 0.003 cm^3 μm m^{-2} 24 h^{-1} kPa^{-1}). In addition, the Gelbo flex test combined with oxygen permeance (PO$_2$) measurements and optical microscopy are firstly reported for evaluating the durability of coatings, revealing that the CNs coated PET and OPA provide the best performance among the investigated coated films. CNs are therefore considered to be a promising multi-functional coating for flexible food packaging.

Keywords Cellulose nanocrystals (CNs) · Food packaging · Oxygen barrier · Anti-fog properties · Bio-coating

F. Li (✉) · L. Piergiovanni
Packaging Division, Department of Food, Environmental and Nutritional Sciences (DeFENS), Università degli Studi di Milano, Via Celoria, 2, 20133 Milan, Italy
e-mail: fei.li@unimi.it

P. Biagioni
Dipartimento di Fisica and CNISM, Politecnico di Milano, Piazza Leonardo da Vinci, 32, 20133 Milan, Italy

M. Bollani
IFN-CNR, L-NESS, Via Anzani 42, 22100 Como, Italy

A. Maccagnan
Packaging Division, GOGLIO S.p.A., Via dell'Industria 7, 21020 Daverio, VA, Italy

Introduction

Nowadays, the vast majority of food packaging materials are constituted of petrol-based plastics, increasing the dependency of the global economy on fossil resources. Therefore, considering also environmental problems, the interest in bio-based materials, such as poly lactic acid (PLA; Vert et al. 1995; Drumright et al. 2000; Auras et al. 2004; Lim et al. 2008), starch (Tharanathan 2003; Avella et al. 2005), gluten (Guillaume et al. 2010; Montaño-Leyva et al. 2013), or other bio-polymers (Cha and Chinnan 2004; No et al. 2007; Rhim and Ng 2007; Hansen and Plackett 2008; Muzzarelli et al. 2012) has recently been hugely rising. However, such materials are not yet widely applicable because of their inferior properties (Ray et al. 2002, 2003; Krikorian and Pochan

2003) and high cost, compared with conventional ones, and still many challenges exist before substituting bio-based materials for conventional plastics.

The use of plastic materials for flexible food packaging also poses a challenge in finding appropriate strategies to improve their barrier properties. In current research, inorganic coating, such as aluminum (Chatham 1996; Lange and Wyser 2003) and SiO_2 (Erlat et al. 1999; Haas et al. 1999; Creatore et al. 2002) or nano-clays fillers (Sánchez-Valdes et al. 2006; Priolo et al. 2010; Ghasemi et al. 2012; Svagan et al. 2012), are used as oxygen or water vapor barriers with inevitable disadvantages that include a tendency to crack (Priolo et al. 2010) and potential health risks (Lordan et al. 2011). Therefore, a sound strategy consists in partially replacing conventional petrol-based plastics with bio-based materials, for instance, utilizing bio-coatings with the twofold aim of improving the original plastic properties and reducing the plastic use. Bio-coatings can, therefore, be considered as one of the suitable solutions for food packaging applications. Nevertheless, the number of directly related bio-coating publications is still limited. Gelatin (Farris et al. 2009) or pullulan (Farris et al. 2012) have been recently reported as oxygen barriers on PET or oriented polypropylene (OPP) plastic films. Isogai and his group (Kato et al. 2005) compared the oxygen barrier properties of 12 μm-thick PET films coated by TEMPO-oxidized microcrystalline cellulose, chitosan and starch, whilst TEMPO-oxidized nano-fiber coatings have been demonstrated as an oxygen barrier on PLA and PET film (Fukuzumi et al. 2009; Fujisawa et al. 2011; Rodionova et al. 2012). Besides cast coating, some research groups successfully improved barrier properties of food packaging materials through layer-by-layer (LbL) assembly (Jang et al. 2008; de Mesquita et al. 2010; Priolo et al. 2010; Zhang and Sun 2010; Yang et al. 2011; Svagan et al. 2012; Li et al. 2013). However, at present TEMPO-oxidized and LbL coating processes are still difficult to apply at the industrial scale due to their cost and process complexity.

In this work, we investigate the mechanical, optical, and barrier properties of a bio-coating made of cellulose nanocrystals (CNs), which can be obtained from the most abundant natural polymer on earth. Besides the promising results that are discussed throughout the paper, such material brings advantages also in terms of low weight, low cost, and

biodegradability. Over the last few years, CNs have been extracted from different original sources by chemical, physical, enzymatic processes, or a combination of them (Siró and Plackett 2010; Yue et al. 2012) and frequently used as a filler into other bulk materials for improving barrier (da Silva et al. 2012; Fortunati et al. 2012; Martinez-Sanz et al. 2012), mechanical (Siqueira et al. 2010; Martinez-Sanz et al. 2012; Zhou et al. 2012), and other properties. To our best knowledge, however, only a limited number of researches focused on CNs cast coating. Herein, we chose a chemical-hydrolysis method for CNs production from cotton linters and we deposited them on different conventional flexible food packaging materials to produce a multi-functional coating. In particular, we report for the first time a systematic analysis for a dispersion of CNs as the coating material deposited on PET, OPP, OPA and cellophane films. The morphology, coefficient of friction, anti-fog, optical, oxygen barrier, and water vapor barrier properties of coated films were measured and systematically interpreted.

Materials and methods

Materials

Cotton linters were provided by S.S.C.C.P. (Milan, Italy) as the raw material to produce CNs.

Four different plastic substrates were coated and used for experiments: (1) poly(ethylene terephthalate) (PET, 12 ± 0.5 μm in thickness), (2) oriented polypropylene (OPP, 20 ± 0.5 μm in thickness), (3) oriented polyamide (OPA, 12 ± 0.5 μm in thickness), and cellophane (CELL, 12 ± 0.5 μm in thickness). All plastic films have been provided by Radici Film, San Giorgio di Nogaro, Italy.

Methods

CNs extraction

1 wt% Cellulose nanocrystals (CNs) dispersion was produced from cotton linter by a procedure described elsewhere (Li et al. 2013). Briefly, milled cotton linters were hydrolyzed by 64 wt% sulfuric acid with vigorous stirring at 45 °C for 45 min. The reaction mixture was diluted with deionized water and then rinsed and

centrifuged at 5,000 rpm repeatedly until the supernatant became turbid. Further purification was then done by dialysis against deionized water (Molecular Weight Cut Off 12 000 and higher). Sequentially, the suspension was sonicated (UP400S 400 W, Hielscher Co., Germany) to create cellulose crystals of colloidal dimensions. Finally, the suspension was filtered under vacuum with Muktell (grade GF/C, 1.2 μm pore diameter) and Whatman glass microfiber filter (grade GF/F, 0.7 μm pore diameter) to remove contamination and big aggregations. The CNs content of the resulting aqueous suspension was determined by drying several samples (1 ml each) at 105 °C for 15 min intervals (to avoid decomposition or burning) until weight constancy, giving a cellulose concentration of ∼1 wt% and a yield of ∼50 %. To prepare a given concentration of CNs solution, the resulting CNs dispersion was adjusted to pH ∼7 by 1 M NaOH(aq), freeze-dried and stored in tightly sealed container under dry conditions for later analysis and experiments.

Particle size distribution

1 wt% CNs dispersion was scanned by a laser diffraction particle size analyzer (Mastersizer 2000; Malvern Instruments), combining a blue source at 470 nm wavelength and a red source at 632.8 nm wavelength.

Preparation of coating dispersion

An 8 wt% CNs water dispersion was obtained by dissolving the CNs into distilled water assisted with ultrasonic treatments until the dispersion became visually homogenous. During the process, the sonication should be carried out every 10 min in water bath to avoid overheating. After recovering to room temperature, the CNs dispersion was coated on different plastic films.

Coated film preparation

According to ASTM D823-07, practice C, the corona-treated sides (external sides) of four different rectangular (25×20 cm^2) plastic films were coated by an automatic film applicator (model 1137, Sheen Instruments, Kingston, UK) at a constant speed of 2.5 mm s^{-1}. Water was evaporated using a constant mild air flow (25 ± 0.3 °C for 5 min) at a perpendicular distance of 40 cm from the automatic applicator. The coated films were stored under controlled conditions (20 ± 2 °C, 50 % RH) for 24 h, and then stored in sealed anhydrous desiccators for 24 h before analysis. All substrates are distinguished by external (Ex) and internal (In) sides. The external side is the pre-treated part, while the internal side is without corona treatments.

Thickness measurements

For the coating thickness measurement, a 10×10 cm^2 sample (plastic substrate with coating) was cut and weighed (m_1, g). The coating was then removed by running hot water (∼70 °C) and the resulting bare film was weighed (m_2, g). The coating thickness (l, μm) was obtained according to the following equation:

$$l = \frac{m_1 - m_2}{\rho} \times 100, \tag{1}$$

where $\rho \sim 1.58$ g cm^{-3} is the density of CNs (Mazeau and Heux 2003). Three measurements were performed for each coating type.

Microscopy

Transmission electron microscopy (TEM) Drops of aqueous dispersions of CNs (0.05 wt%) were deposited on carbon-coated electron microscope grids, negatively stained with uranyl acetate and allowed to dry. The samples were analyzed with a Hitachi Jeol-10084 TEM operated at an accelerating voltage of 80 kV.

Atomic force microscopy (AFM)

AFM topography images have been acquired in tapping mode with a Veeco Innova instrument. Super-sharp silicon probes (typical radius of curvature 2 nm) have been used for high-resolution imaging of nanocrystals, while standard silicon probes have been employed for large-area scans in order to evaluate the sample roughness.

The root mean square roughness S is calculated as the standard deviation of the topography ($M \times N$ pixels):

$$S = \sqrt{\frac{1}{MN} \sum_{i=1}^{M} \sum_{j=1}^{N} \left| z(x_i, y_j) - \bar{z} \right|^2}, \qquad (2)$$

where $\bar{z}$ is the mean value of the topography $z(x, y)$.

Optical microscopy

Gelbo Flex treated CNs coated samples were observed using an optical microscope (Micro Nikon Eclipse ME600 Laboratory Imaging; Nikon Instruments, Sesto Fiorentino, Italy) at 5× and 10× magnification. Pieces of film (30 × 30 mm^2) were mounted on a rectangular glass sample holder and observed without any pretreatment. Images were captured by NIS-Element software (Nikon Instruments, Sesto Fiorentino, Italy).

Coefficient of friction

The static (μ_S) and dynamic (μ_d) friction coefficients were measured by a dynamometer (model Z005, Zwick Roell, Ulm, Germany), in accordance with the standard method ASTM D 1894-87. Firstly, the uncoated side of CNs coated film was attached on a specific sled (6.2 × 6.2 cm^2, 197.99 g), while the bare film was covered on the sliding plane. Then the sled was connected to the force sensor of dynamometer. At the end the sled was horizontally pulled by the instrument on the covered sliding plane, while the raw data (pulling force) were recorded and analyzed by software TestXpert V10.11 (Zwick Roell, Ulm, Germany).

Optical properties

Transparency The specular transmittance of the sample was measured at a wavelength of 550 nm, according to the ASTM D 1746-70, by means of a spectro-photometer equipped with 150 mm integrating sphere (model L650, Perkin-Elmer, Milano, Italy).

Haze Haze was measured in accordance with ASTM D 1003-00 by means of the same instrument for transparency as above. The haze values of uncoated and coated films were obtained as:

$$haze = 100 \times \frac{T_d}{T_t}, \qquad (3)$$

where T_d and T_t are the diffuse and total transmittance, respectively.

Anti-fog test

The boiling test was established and modified from the European Standard test (EN168). In this test, a coated film was placed on top of a white container with hot water (95 °C) and a black sponge. The black sponge was observed through the film by naked eye after the film was exposed to the steam from the white container. The visibility of the black sponge was empirically evaluated for anti-fog performance.

Contact angle measurements

Contact angles were measured to estimate the surface energies of the tested substrates by OCA 15 Plus angle goniometer (Data Physics Instruments GmbH, Filderstadt, Germany). The software (SCA20 and SCA21) provided by the instrument manufacturer calculate the surface energy based on contact angles measurements. Measurements of static and advancing contact angle were performed at room temperature with two polar liquids and one apolar liquid: Milli-Q water, formamide (FOM, ≥99.5 %, Carlo Erba, Milano, Italy), and diiodomethane (DIM, 99 %, Sigma Aldrich), respectively. Each measurement was repeated on at least five different positions for each sample. The surface energies were calculated from the contact angle data at equilibrium by the van Oss method (van Oss 2006), which divides the total surface free energy into two components, the dispersive and the polar components, where the polar interactions originate from the Lewis acid–base interactions:

$$\gamma_i^{total} = \gamma_i^D + \gamma_i^P, \qquad (4)$$

where

$$\gamma_i^P = 2\sqrt{\gamma_i^+ \gamma_i^-}, \qquad (5)$$

The subscripts i indicate the solid ($i = s$) or liquid ($i = l$) phase, and the superscripts refer to the dispersive (D) and polar (P) components of the total surface energy. γ^+ and γ^- are electron-acceptor and donor parts of the Lewis acid–base interactions.

When combined with Young's equation, the equations developed by Chaudhury, Good, and van Oss yield the equation (van Oss 2006)

$$\gamma_l(1 + \cos\theta) = 2\left(\sqrt{\gamma_l^D \gamma_s^D} + \sqrt{\gamma_s^+ \gamma_l^-} + \sqrt{\gamma_s^- \gamma_l^+} \right), (6)$$

where θ is the contact angle, γ_l is the liquid surface tension (mJ m^{-2}), and γ_s^+, γ_s^- and γ_l^+, γ_l^- are electron-

Table 1 Surface tension components and parameters of the liquids used in direct contact angle determination in mJ m^{-2}, at 20 °C (van Oss 2003)

Liquid	γ_l	γ_l^D	γ_l^P	γ_l^+	γ_l^-
Apolar					
Diiodomethane	50.8	50.8	0	≈ 0.01	0
Polar					
Water	72.8	21.8	51.0	25.5	25.5
Formamide	58.0	39.0	19.0	2.28	39.6

acceptor and donor contributions to the polar component of the solid and liquid, respectively (mJ m^{-2}). The values of the surface tension and its components for each liquid used in calculations were found in literature (van Oss 2003). Water, formamide, and diiodomethane, with known γ_l^D, γ_l^+, and γ_l^- values (9 known parameters, Table 1) and measured contact angle (θ) (3 known parameters) were used to determine γ_s^D, γ_s^+, and γ_s^- (only 3 unknown parameters) combined with Eq. (6) (15 parameters). Finally, γ_s^{total} and γ_s^P were calculated from Equation (4) and (5).

Oxygen and water vapor permeance (PO$_2$ and PH$_2$O) measurements

The PO$_2$ and PH$_2$O of CNs coated plastic films were measured by permeation instruments (MOCON, OX-TRAN® model 702 and PERMATRAN-W® model 700) at 23 °C and 0 % relative humidity (RH) and at 38 °C and 100 % RH difference, complying with ASTM D-3985, F-1927, F-1307 and ASTM F-1249, respectively.

The PO$_2$ of the CNs coating in the coated film [i.e., PO$_2$(Coating)] was calculated using the following equation:

$$\frac{1}{\text{PO}_2(\text{coating})} = \frac{1}{\text{PO}_2(\text{coated film})} - \frac{1}{\text{PO}_2(\text{film})}, \quad (7)$$

where PO$_2$(coated film) and PO$_2$(film) are the oxygen permeance (cm^3 m^{-2} 24 h^{-1} kPa^{-1}) for the coated substrate and the bare substrate, respectively.

Gelbo flex testing

According to a slightly modified ASTM F392 standard, the CNs coated samples were mounted on the
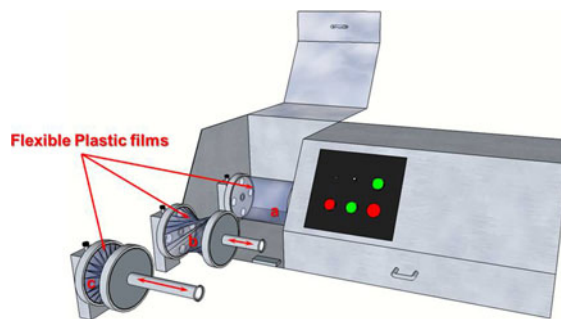
Fig. 1 Gelbo Flex tester, *a*, *b*, and *c* indicate different phases of a back and forth cycle

Gelbo flex tester (model S/N 80 03 32, VINATORU ENTERPRISES INC, Graham, USA) as depicted in the 'a' status in Fig. 1 and then treated by 20 cycles as shown in the 'b–c' status in the same figure. Each cycle includes back and forth twisting by 440° of the mounted film. The samples were observed by optical microscopy after treatments and the oxygen permeance was measured before and after treatment to evaluate the durability of CNs coating on different substrates by the method described above.

Results and discussion

Morphology

The rod-like CNs produced by sulfuric acid hydrolysis of cotton linters were characterized by TEM as shown in Fig. 2. CNs observations obtained from casted diluted dispersion (approximate 0.05 wt%) show individual nanocrystals and some aggregates. The appearance of aggregated elementary crystallites in TEM images is expected due to the high specific area and strong hydrogen bonds established between the CNs. From several TEM images, the mean values of the length (L) and diameter (d) of the isolated CNs were determined to be 120 ± 30 and 6 ± 3 nm, respectively, giving an aspect ratio (L/d) ~ 20. Similar dimensions have been reported in the literature (Angles and Dufresne 2000; Elazzouzi-Hafraoui et al. 2007). In order to better understand the CNs size distribution, the probability histogram for the particle size distribution of 1 wt% CNs dispersion is shown in Fig. 3. It indicates that the range of the CNs length is from 90 to 160 nm (mean value ~ 115 nm), which is highly similar with the results obtained from TEM
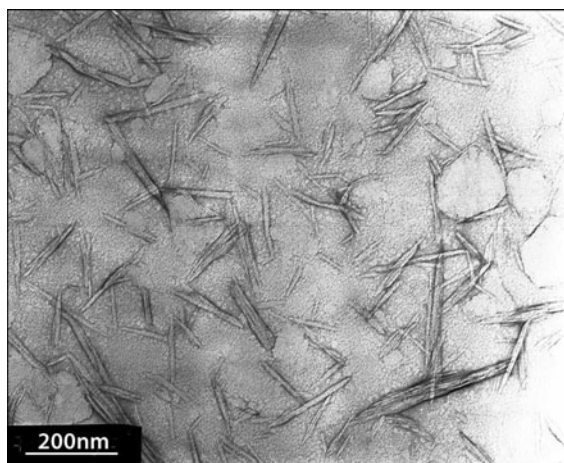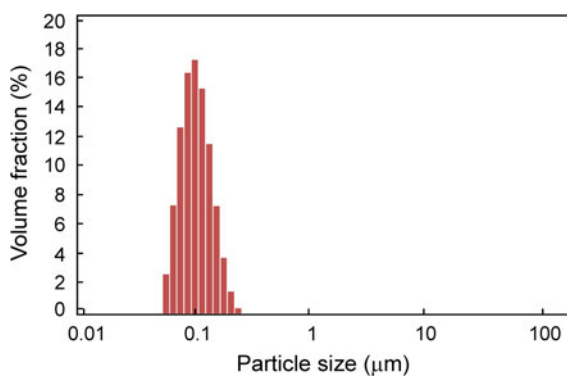
Fig. 2 TEM image of individual CNs

Fig. 3 Probability histogram for the particle size distribution measured from 1 wt% CNs dispersion

(Fig. 2) and by other authors (Habibi et al. 2010). A certain degree of size distribution is inevitable owing to the acid diffusion-controlled nature of the hydrolysis (de Mesquita et al. 2010). However, the results demonstrate that the acidic hydrolysis process is highly reliable and effective to extract relatively uniform CNs from cotton linters.

Figure 4 shows high-resolution AFM images of CNs coated films. The image shows a dense packing and uniform coverage of nanofibers. We therefore conclude that a new CNs layer was homogeneously established on different conventional packaging materials. Dense packing of CNs has been previously described in other reports (Fujisawa et al. 2011). The continuous layer of overlapping CNs fibers (Siró and Plackett 2010) points towards possible improvements of the oxygen barrier properties of the different
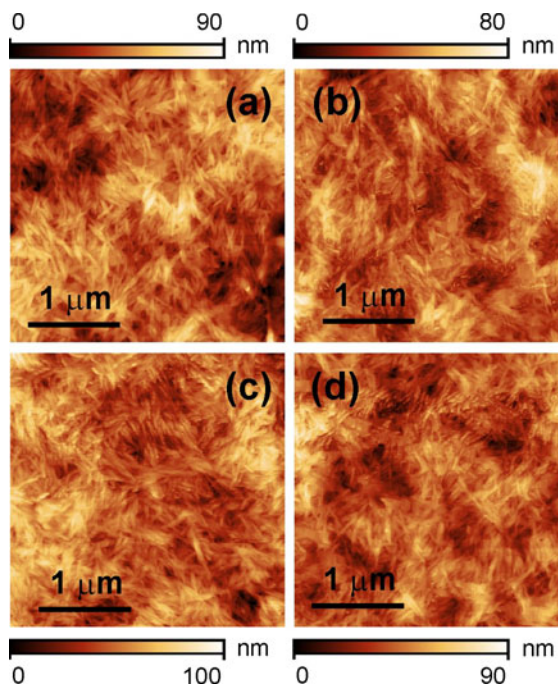

Fig. 4 High-resolution AFM images of CNs coated PET (**a**), OPP (**b**), OPA (**c**), and CELL (**d**)

substrates, which we will demonstrate and discuss later on. Moreover, we acquired large-area AFM images, as shown in Fig. 5, where CNs cobble-stone pathway-like aggregations appear due to the strong hydrogen bonds. All images are qualitatively very similar with each other. Root-mean-square roughness values calculated from such AFM investigations all lay in a low-value range (6–13 nm), which is definitely more narrow than the one measured for the external side of bare films (2–21 nm, not shown). A low roughness has been correlated to a less opportunity for biofilm formation (Shellenberger and Logan 2001; Li and Logan 2004; Ringus and Moraru 2013), thus bacterial fouling occurrence can be likely reduced by such a coating when applied onto rough substrates.

Coefficient of friction (COF)

The values for the coefficient of friction (COF) of CNs coated films against films are presented in Table 2. By means of the statistical analysis, we again can conclude that the casting deposition created a completely new CNs-coating layer on different substrates with one exception. In fact, it can be clearly noted that three of the investigated systems (coated PET, OPA,
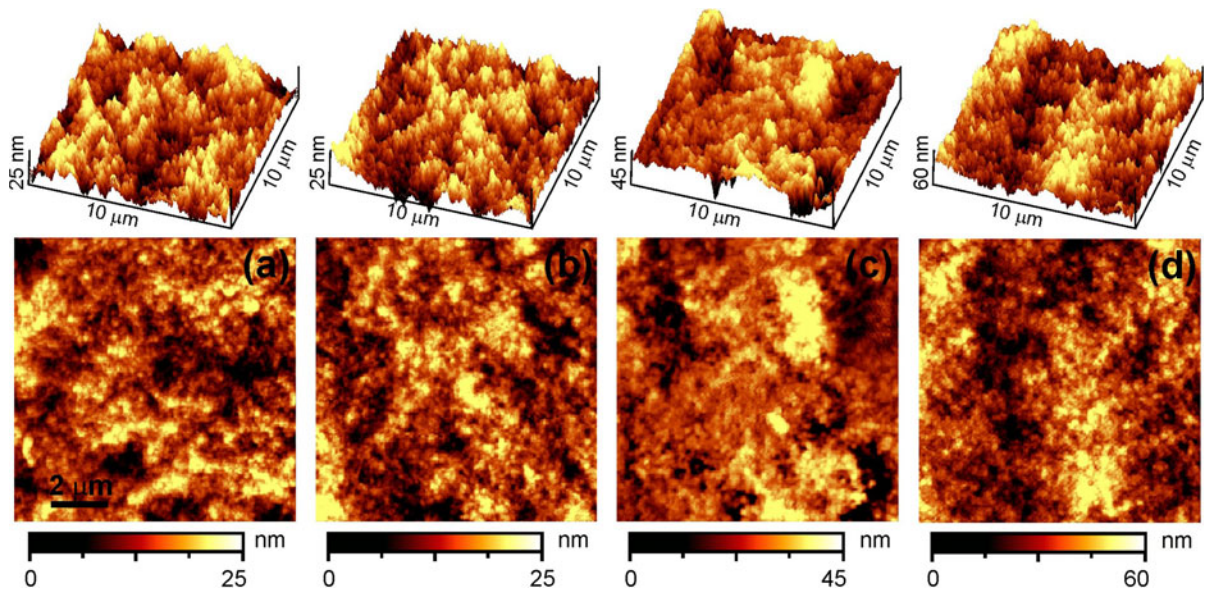
Fig. 5 AFM for roughness of CNs coated substrates, coated PET (**a**), OPP (**b**), OPA (**c**), and cellophane (**d**)

Table 2 The coefficient of friction (COF) of Plastic films (Ex) against plastic film (In)

Substrate	Bare (Ex)		Coated (600 nm[a])	
	μ_s	μ_d	μ_s	μ_d
PET	0.57 ± 0.02^D	0.52 ± 0.03^H	0.38 ± 0.01^C	0.33 ± 0.01^G
OPP	0.18 ± 0.01^A	0.17 ± 0.00^F	0.30 ± 0.02^B	0.18 ± 0.01^F
OPA	0.79 ± 0.02^E	$0.74 \pm 0.03^{\,J}$	0.32 ± 0.01^{BC}	0.32 ± 0.02^G
CELL	0.62 ± 0.03^D	0.57 ± 0.01^I	0.38 ± 0.02^C	0.34 ± 0.01^G

[A–E] Different letters mean that static COFs are significantly different ($p < 0.01$)

[F–J] Different letters mean that dynamic COFs are significantly different ($p < 0.01$)

[a] Thickness of CNs coating

and CELL) present similar values in dynamic (μ_d) COFs, while only CNs coated OPP is significantly different from the other coated films and close to the bare one, probably due to weak adhesion between CNs coating and OPP surface which leads to the removal of CNs from substrate during dynamic measurements. To the best of our knowledge, only a limited number of researches focused on the COF property of CNs so far. Hoeger et al. reported that COF of CNs layer-by-layer coating with interlayer Poly(ethyleneimine) is 0.51 ± 0.23 with 1 μm scratch length (Hoeger et al. 2011). Their COF values obtained by nano-indentation are larger than our mean values (0.34 ± 0.02) obtained by dynamometery because of the different contact materials (bare films against CNs coating or diamond tip against CNs coating) and coating methods (cast and layer-by-layer coating). Moreover, the COF results, AFM figures, and oxygen permeance discussed later indicate that for thin CNs coating a homogenous independent layer was established by cast coating. It is thus concluded that CNs coating results in an improvement for practical applications, because of the reduction of friction between the films, which might represent a premium feature for high-speed packaging machineries.

Optical properties

As for optical properties, the transparency and haze values of bare films are 87–92 and 2.1–3.0 %,

respectively, while the ones of coated films are 88–91 and 3.3–4.0 %. Detailed results in Table 3 show that the CNs coated films still maintain high transparency and low haze, as requested to ensure easy evaluation of the product quality inside the package. In other words, the changes of transparency and haze of CNs coated films remain within ~1 %. Overall, the thin CNs coating (~1.5 μm, determined by weighting the samples) has no significant influences on the optical properties of coated films.

Anti-fog properties

Besides the COF improvements and maintaining excellent optical properties, empirical boiling water test both showed that the CNs coated films have excellent anti-fog properties, which are presented in Fig. 6. Particularly, these properties are achieved by just using biopolymers instead of chemical additives included in the plastic film for which CNs coating indicates high potential of substitution. In Fig. 6 we show the results for the coated OPP film only, since OPP is the most hydrophobic material among the substrates under investigation, but very similar results were obtained for all the substrates. We observed the border [blue dashed line in panels (b) and (c)] between

bare and coated films by eye inspection. In order to better observe the anti-fog property, we set a black sponge in the water containers, as shown in Fig. 6b. As known, fog is formed by small discontinuous water droplets that diffuse the incident light, thereby decrease the transparency and increase the haze (Nuraje et al. 2010; Introzzi et al. 2012). Figure 6c, obtained with optical microscopy, presents two parts, an uncoated one with water droplets, which forms fog, and a coated one with a homogeneous water layer without any droplets, which remained transparent. In the following part, we will further interpret the excellent anti-fog properties of CNs coated films from the comparison of surface energies obtained from contact angle goniometry.

From Tables 4 and 5, we could notice that the CNs coated films show highly similar static contact angles, which indicates that a completely new CNs layer was established through cast coating process. The static contact angles of CNs coated substrates are much lower than the ones of bare substrates, since cellulose chains contain many hydroxyl (-OH) groups leading to its hydrophilicity. Meanwhile, the dynamic contact angles, which might better reveal the real behavior of

Table 3 Transparency at 550 nm and haze of bare and CNs coated films

Substrates	Transparency (%)		Haze (%)	
	Bare	CNs coated	Bare	CNs coated
PET	87.5 ± 0.3	89.0 ± 0.3	2.9 ± 0.1	3.3 ± 0.2
OPP	91.8 ± 0.0	90.8 ± 0.2	2.1 ± 0.0	3.4 ± 0.3
OPA	90.2 ± 0.5	89.8 ± 0.0	3.0 ± 0.1	4.0 ± 0.2
Cellophane	87.3 ± 0.1	88.3 ± 0.1	3.2 ± 0.1	3.8 ± 0.2

Table 4 Static contact angles of bare and CNs coated films

Films	Static CA[a]		
	$\theta_{Water}(°)$	$\theta_{DIM}(°)$[b]	$\theta_{FOM}(°)$[c]
Bare PET	57.44 ± 5.84	22.41 ± 2.73	39.55 ± 1.77
Bare OPP	63.03 ± 1.00	52.22 ± 1.61	41.39 ± 1.70
CNs-PET	12.32 ± 1.33	37.15 ± 3.02	7.41 ± 1.33
CNs-OPP	12.08 ± 0.95	36.37 ± 1.70	8.78 ± 0.73

[a] Static contact angle values recorded at 60th second

[b] DIM, diiodomethane
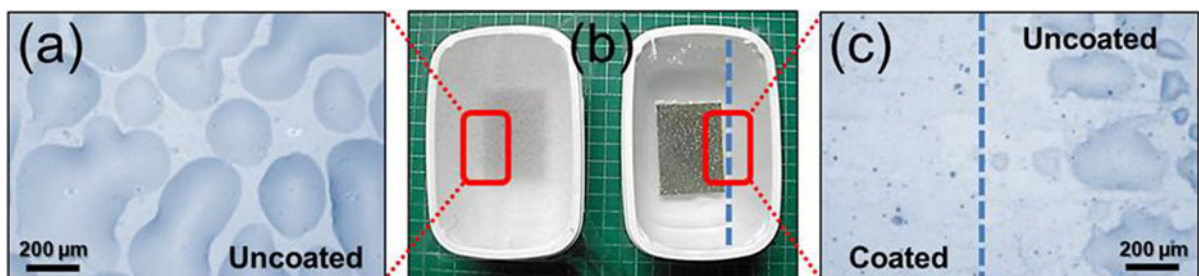
[c] FOM, formamide

Fig. 6 Boiling water test; panel (**a**) the foggy bare OPP observed with an optical microscope; panel (**b**) comparison between bare and CNs coated OPP during the test; panel (**c**) the border between CNs coated and bare parts observed with an optical microscope

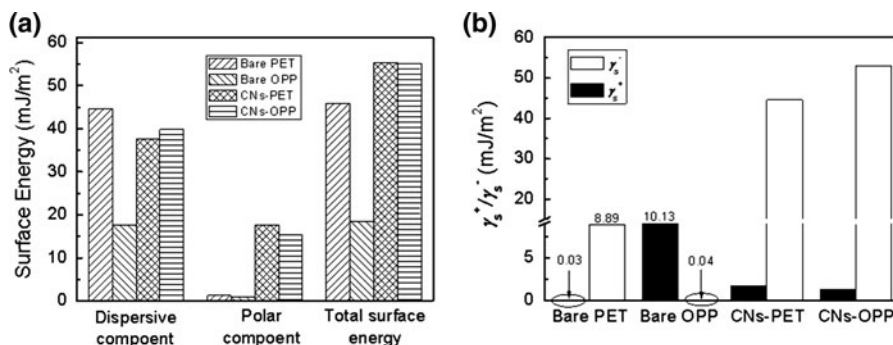**Table 5** Advancing and receding contact angles of bare and CNs-coated films

Films	Advancing CA[a]			Receding CA[a]		
	$\theta_{Water}(°)$	$\theta_{DIM}(°)$[b]	$\theta_{FOM}(°)$[c]	$\theta_{Water}(°)$	$\theta_{DIM}(°)$[b]	$\theta_{FOM}(°)$[c]
Bare PET	72.57 ± 2.96	29.00 ± 2.12	50.27 ± 2.97	25.34 ± 2.12	8.16 ± 0.82	14.30 ± 2.76
Bare OPP	90.06 ± 1.84	79.72 ± 0.69	52.99 ± 2.65	17.18 ± 3.41	22.72 ± 1.26	11.23 ± 1.38
CNs-PET	26.29 ± 3.27	43.91 ± 2.03	17.10 ± 0.74	8.56 ± 2.23	8.20 ± 0.34	6.79 ± 2.01
CNs-OPP	27.33 ± 3.07	39.56 ± 2.50	17.30 ± 2.94	5.63 ± 0.45	7.21 ± 4.63	5.58 ± 2.33

[a] Dynamic contact angle values

[b] DIM, diiodomethane

[c] FOM, formamide

Fig. 7 Surface energies and their respective polar and dispersive components of bare and CNs coated PET and OPP (**a**), the electron-acceptor and donor of polar component (**b**)

hydrophilic surfaces, were also determined. Moreover, it was reported that the differences between the advancing and receding contact angles are usually related with surface's roughness and water absorption often observed on natural fibers (Dankovich and Gray 2011).

We used contact angles combined with surface energies of CNs coating to interpret the principles behind the anti-fog performance. The static and dynamic contact angle values (Tables 4, 5) are in good agreement with results recently presented on nano-cellulose coated or casted films (Dankovich and Gray 2011). Regarding the anti-fog properties, it was reported that one possible measure of the level of interaction of water with a material is the advancing contact angle and it has been suggested that hydrophilic surfaces with contact angles lower than 40° should exhibit anti-fog behavior (Briscoe and Galvin 1991; Howarter and Youngblood 2008). Indeed, the measured advancing contact angle values (θ_{Water}) of CNs coated films are about 26–27°.

To further interpret the anti-fog behavior, we calculated the surface energies values from contact

angles, presented in Fig. 7. In the literature, the surface energy of cellulose determined by contact angle measurements is known to be ∼55 mJ m^{-2} (Aulin et al. 2009). Also, a value for the surface energy of CNs films on different substrates was reported as high as 65 mJ m^{-2} with ±15 % experimental error (Kontturi et al. 2007). These values are consistent with the values obtained in our results of CNs coated PET and OPP. In this paper, we limited our research on these two substrates only, since PET and OPP are the most commonly used films for food packaging and are very different in polarities. Contact angles were measured by using water, FOM, and DIM to provide information regarding the contributions of dispersive (D) and polar (P) components to the total surface energy of the substrates. The calculated values in Fig. 7a indicate that the dispersive part of the CNs surface energy is larger than the polar contribution as well as the CNs hydrophilic property, we thus further investigate the electron-acceptor and donor components to the polar part of total surface energy shown in Fig. 7b. From Fig. 7b, bare PET and OPP have different asymmetric electron-acceptor and donor

patterns due to PET and OPP being relatively hydrophilic and hydrophobic, respectively, while the CN-coated PET and OPP have similar asymmetric patterns which disclose that the thin CNs coating results in an independent and homogeneous layer on PET and OPP substrates. This is a common occurrence since, for a given polar substrate, a strong asymmetry is usually observed between the contribution of electron-acceptor and electron-donor interactions, making one of the two dominant (van Oss 2006). Furthermore, the electron-donor component (γ_s^-) values of coated PET and OPP shown in Fig. 7b are at least 5 and 2,000 times the bare ones, which is likely the fundamental factor for different anti-fog performances between bare and coated films. Also, cellulose always presents a polar and hydrophilic surface (Moon et al. 2011) and CNs are grafted with a few sulfate ester groups ($-O-SO_3^-$) due to the sulfuric acid hydrolysis process. These results, therefore, suggest that the anti-fog property induced on the PET and OPP substrates should be attributed to the electron-donor parameter of the polar component. For hydrophilic biopolymers, similar results were also reported (Nuraje et al. 2010; Introzzi et al. 2012).
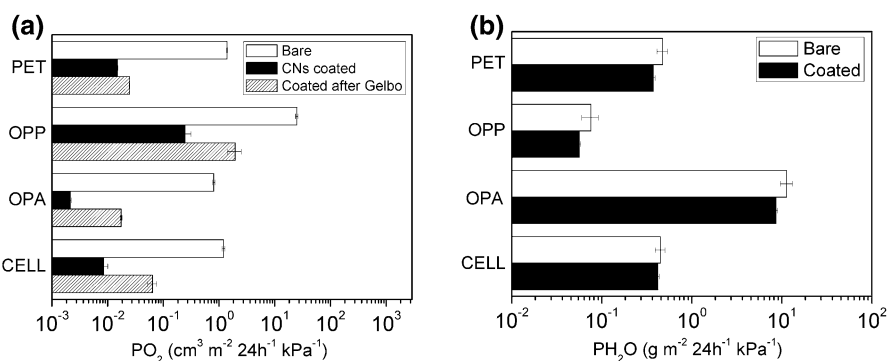
Barrier properties

In addition to excellent performances on COF, optical, and anti-fog properties, the CNs barrier function is evaluated as follows. Figure 8a shows that the oxygen barrier properties of coated films improve significantly thanks to the thin (1.5 μm) CNs coating. The coatings allow for a dramatic reduction (>99 %) of oxygen permeance (PO_2) of all CNs coated samples. According to our best knowledge, this is the first systematic report on PO_2 of CNs coated films. Such excellent

oxygen barrier properties achieved on different substrates can be tentatively attributed to the strong hydrogen bonds among CNs and the dense packing of the coating applied. Furthermore, we also calculated the oxygen permeability coefficients ($P'O_2$) of CNs coating only as follows: 0.02 on PET, 0.37 on OPP, 0.003 on OPA, and 0.01 on CELL (cm^3 μm m^{-2} 24 h^{-1} kPa^{-1}), finding always very low values. In particular, $P'O_2$ of CNs coating on OPA is down to 0.003 cm^3 μm m^{-2} 24 h^{-1} kPa^{-1}, which is much lower than that of commercialized oxygen barrier, ethylene vinyl alcohol (EVOH), under dry condition (Lee et al. 2008). Also, this $P'O_2$ value is comparable with the best oxygen barrier from wood TEMPO-oxidized cellulose nanofiber (TOCN-COONa; Fukuzumi et al. 2011). Therefore, our results indicate that CNs coating provides very good oxygen barrier (especially under dry conditions) but also that, because of the differences in calculated $P'O_2$ for CNs coating applied on diverse surfaces, the effectiveness of this property is related to the possible interactions between CNs and different substrates. One more interesting point is the achievement of high oxygen barrier using short CNs ($\sim$120 nm). In other words it seems to be demonstrated that long entangled cellulose fibers (Belbekhouche et al. 2011) are not the only crucial point in achieving high oxygen barrier. In the following Gelbo flex test part, the effects of affinity between CNs and substrates on oxygen barrier properties will be further discussed.

Gelbo flex test is intended to stress extensively the permeable surfaces for evaluating the durability and coating adhesion strength. The PO_2 of CNs coated films after Gelbo Flex test is also presented in Fig. 8a. As known (Habibi et al. 2008; Isogai et al. 2011; Moon et al. 2011), nano-cellulose is stiff and rigid, which

Fig. 8 The oxygen permeance (PO_2) of bare, CNs coated, and CNs coated after Gelbo Flex tests PET, OPP, OPA, and CELL films at 23 °C under dry condition (**a**); the water vapor permeance of bare and CNs coated PET, OPP, OPA, and CELL films at 38 °C under 100 % RH difference (**b**)

should result in fragility of the coating and, thereby, a possible partial loss of the gas barrier properties during usage. Meanwhile, from our results (data not shown), bare and CNs coated films has similar mechanical property (Young's modulus and elongation limit). In other words, the rigid thin CNs coating cannot significantly affect final mechanical performance. Based on the above considerations, we compared the oxygen barrier before and after Gelbo Flex tests. The results indicate that strong distortions led to some destructions of CNs coating and reduce the oxygen barrier properties of all CNs coated films. Gelbo Flex treated CNs coated PET and OPA films, however, still maintain a significant low PO_2. Compared with others, Gelbo Flex treated coated OPP and cellophane films show relatively higher PO_2, probably due to their weak adhesion, which was also observed in dynamic COF tests especially for OPP. In order to confirm this point, we did observations by optical microscopy and the figures are presented in Fig. 9. The morphologies of PET and OPA in Fig. 9a and c reveal better adhesions between CNs and PET and OPA, since only a very small portion of the CNs film was peeled off from substrates even though there are many chaps (crackles) especially at strongly twisted parts of CNs

coatings. However, in case of Gelbo Flex treated CNs coated OPP, from Fig. 9b we found cracked coating parts and refractive light through the coating indicating that the coating is likely separated from the OPP (seems like blister on substrate), which probably results in the observed lower oxygen barrier properties. Blistered and cracked coating also unexpectedly occurred to cellophane, as shown in Fig. 9d. This phenomenon might be explained by the presence of resins coated or laminated on the commercialized cellophanes. The images from optical microscopy are therefore consistent with the lower oxygen barrier on Gelbo Flex treated coated OPP and cellophane. In this work, the oxygen permeance values were measured only under the dry condition. Since CNs is a hydrophilic biopolymer, the oxygen barrier will be certainly reduced under high RH as other paper reported (Fukuzumi et al. 2012). This limitation is common to the currently used synthetic barrier polymers (polyamide (PA), polyvinyl alcohol (PVOH), ethylene vinyl alcohol (EVOH)) and led to the development of multilayer structures (Li et al. 2013), designed in order to protect moisture sensitive polymers with polyolefin such as low-density polyethylene (LDPE), high-density polyethylene (HDPE), and polypropylene (PP).
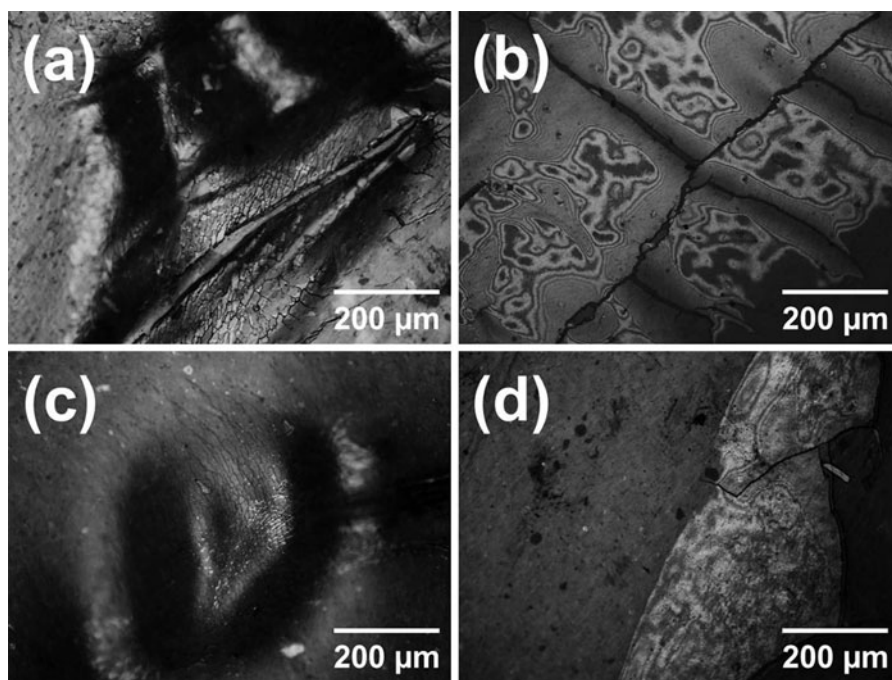

Fig. 9 The morphology of Gelbo Flex treated CNs coated PET (**a**), OPP (**b**), OPA (**c**), and CELL (**d**) films by optical microscopy

The four coated films were also evaluated for their water vapor permeance (PH$_2$O) and Fig. 8b reports the results obtained. The PH$_2$O of CNs coated PET, OPP, OPA and CELL films is reduced by 22, 26, 24 and 6.5 % respectively, compared to bare films, while the corresponding thickness increase is 7.5 % for OPP and 12.5 % for the other three films. Such a limited improvement of the moisture barrier is due to CNs hydrophilicity (Hult et al. 2010; Sanchez-Garcia et al. 2010; Moon et al. 2011) and also to the heavy conditions of the test used (38 °C under a difference of 100 % RH). However, the water vapor barrier properties of CNs coating might be satisfactory in real-use conditions which generally involve lower temperature and RH values. Also, high water vapor barrier can already be achieved by conventional and convenient synthetic polymers such as PP and PE.

Conclusions

To the best of our knowledge, this is the first time that CNs are deposited on different substrates as multi-functional coatings. In the literature, CNs are usually considered as a filler (Noorani et al. 2007; Habibi et al. 2008; Siqueira et al. 2010; Goffin et al. 2011; Dong et al. 2012) or used for small-scale spin or layer-by-layer coating (Kontturi et al. 2007; Cranston and Gray 2008; Cerclier et al. 2010; Hoeger et al. 2011; Li et al. 2013), and are assumed not to function as a practical coating material (Isogai et al. 2011). In this paper, we systematically investigated the properties of conventional films coated with CNs, demonstrating that CNs coatings mainly lead to a reduction of friction, a premium feature for industrial applications, and that they do not influence significantly the optical properties of coated films. Moreover, CNs coating shows excellent anti-fog property, which is a strongly required performance for flexible food packaging, intended to be used for fresh food. Finally, CNs coatings not only dramatically improve the oxygen barrier properties of conventional flexible food packaging material, but also lead to a certain reduction in the water vapor permeance. While substitution of conventional plastics might still be far ahead because of their low cost, large flexibility and availability, the perspective use of CNs as multi-functional coatings to favor a reduction of the required thickness for plastic films, towards a more environmentally-friendly and sustainable approach to packaging seems promising and feasible. The best substrate to be covered with CNs appeared to be PET and OPA films due to their intrinsic polarity and high surface energies; however, the possible use of activation treatments and other plastic substrates remain to be deeply investigated, as well as the possible measures to reduce the moisture sensitivities and mechanical rigidity of the thin nano-cellulose coatings.

References

Angles MN, Dufresne A (2000) Plasticized starch/tunicin whiskers nanocomposites. 1. Structural analysis. Macro-molecules 33:8344–8353

Aulin C, Ahola S, Josefsson P, Nishino T, Hirose Y, Österberg M et al (2009) Nanoscale cellulose films with different crystallinities and mesostructures—their surface properties and interaction with water. Langmuir 25:7675–7685

Auras R, Harte B, Selke S (2004) An overview of polylactides as packaging materials. Macromol Biosci 4:835–864

Avella M, De Vlieger JJ, Errico ME, Fischer S, Vacca P, Volpe MG (2005) Biodegradable starch/clay nanocomposite films for food packaging applications. Food Chem 93:467–474

Belbekhouche S, Bras J, Siqueira G, Chappey C, Lebrun L, Khelifi B et al (2011) Water sorption behavior and gas barrier properties of cellulose whiskers and microfibrils films. Carbohydr Polym 83:1740–1748

Briscoe BJ, Galvin KP (1991) The effect of surface fog on the transmittance of light. Sol Energy 46:191–197

Cerclier C, Cousin F, Bizot H, Moreau C, Cathala B (2010) Elaboration of spin-coated cellulose-xyloglucan multilay-ered thin films. Langmuir 26:17248–17255

Cha DS, Chinnan MS (2004) Biopolymer-based antimicrobial packaging: a review. Crit Rev Food Sci Nutr 44:223–237

Chatham H (1996) Oxygen diffusion barrier properties of transparent oxide coatings on polymeric substrates. Surf Coat Technol 78:1–9

Cranston ED, Gray DG (2008) Birefringence in spin-coated films containing cellulose nanocrystals. Colloids Surf a-Physicochem Eng Aspects 325:44–51

Creatore M, Palumbo F, d'Agostino R (2002) Deposition of SiOx films from hexamethyldisiloxane/oxygen radiofre-quency glow discharges: process optimization by plasma diagnostics. Plasmas Polym 7:291–310

da Silva JBA, Pereira FV, Druzian JI (2012) Cassava starch-based films plasticized with sucrose and inverted sugar and reinforced with cellulose nanocrystals. J Food Sci 77:N14–N19

Dankovich TA, Gray DG (2011) Contact angle measurements on smooth nanocrystalline cellulose (I) thin films. J Adhes Sci Technol 25:699–708

de Mesquita JP, Donnici CL, Pereira FV (2010) Biobased nanocomposites from layer-by-layer assembly of cellulose nanowhiskers with chitosan. Biomacromolecules 11:473–480

Dong H, Strawhecker KE, Snyder JF, Orlicki JA, Reiner RS, Rudie AW (2012) Cellulose nanocrystals as a reinforcing material for electrospun poly(methyl methacrylate) fibers: formation, properties and nanomechanical characterization. Carbohydr Polym 87:2488–2495

Drumright RE, Gruber PR, Henton DE (2000) Polylactic acid technology. Adv Mater 12:1841–1846

Elazzouzi-Hafraoui S, Nishiyama Y, Putaux J-L, Heux L, Dubreuil F, Rochas C (2007) The shape and size distribution of crystalline nanoparticles prepared by acid hydrolysis of native cellulose. Biomacromolecules 9:57–65

Erlat AG, Spontak RJ, Clarke RP, Robinson TC, Haaland PD, Tropsha Y et al (1999) SiOx gas barrier coatings on polymer substrates: morphology and gas transport considerations. J Phys Chem B 103:6047–6055

Farris S, Introzzi L, Piergiovanni L (2009) Evaluation of a biocoating as a solution to improve barrier, friction and optical properties of plastic films. Packag Technol Sci 22:69–83

Farris S, Introzzi L, Fuentes-Alventosa JM, Santo N, Rocca R, Piergiovanni L (2012) Self-assembled pullulan-silica oxygen barrier hybrid coatings for food packaging applications. J Agric Food Chem 60:782–790

Fortunati E, Peltzer M, Armentano I, Torre L, Jimenez A, Kenny JM (2012) Effects of modified cellulose nanocrystals on the barrier and migration properties of PLA nano-biocomposites. Carbohydr Polym 90:948–956

Fujisawa S, Okita Y, Fukuzumi H, Saito T, Isogai A (2011) Preparation and characterization of TEMPO-oxidized cellulose nanofibril films with free carboxyl groups. Carbohydr Polym 84:579–583

Fukuzumi H, Saito T, Wata T, Kumamoto Y, Isogai A (2009) Transparent and high gas barrier films of cellulose nanofibers prepared by TEMPO-mediated oxidation. Biomacromolecules 10:162–165

Fukuzumi H, Saito T, Iwamoto S, Kumamoto Y, Ohdaira T, Suzuki R et al (2011) Pore size determination of TEMPO-oxidized cellulose nanofibril films by positron annihilation lifetime spectroscopy. Biomacromolecules 12:4057–4062

Fukuzumi H, Saito T, Isogai A (2012) Influence of TEMPO-oxidized cellulose nanofibril length on film properties. Carbohydr Polym. doi:10.1016/j.carbpol.2012.04.069

Ghasemi H, Carreau PJ, Kamal MR, Tabatabaei SH (2012) Properties of PET/clay nanocomposite films. Polym Eng Sci 52:420–430

Goffin AL, Raquez JM, Duquesne E, Siqueira G, Habibi Y, Dufresne A et al (2011) From interfacial ring-opening polymerization to melt processing of cellulose nanowhisker-filled polylactide-based nanocomposites. Biomacromolecules 12:2456–2465

Guillaume C, Pinte J, Gontard N, Gastaldi E (2010) Wheat gluten-coated papers for bio-based food packaging: structure, surface and transfer properties. Food Res Int 43:1395–1401

Haas KH, Amberg-Schwab S, Rose K, Schottner G (1999) Functionalized coatings based on inorganic-organic polymers (ORMOCER (R) s) and their combination with vapor deposited inorganic thin films. Surf Coat Technol 111:72–79

Habibi Y, Goffin AL, Schiltz N, Duquesne E, Dubois P, Dufresne A (2008) Bionanocomposites based on poly(epsilon-caprolactone)-grafted cellulose nanocrystals by ring-opening polymerization. J Mater Chem 18:5002–5010

Habibi Y, Lucia LA, Rojas OJ (2010) Cellulose nanocrystals: chemistry, self-assembly, and applications. Chem Rev 110:3479–3500

Hansen NML, Plackett D (2008) Sustainable films and coatings from hemicelluloses: a review. Biomacromolecules 9:1493–1505

Hoeger I, Rojas OJ, Efimenko K, Velev OD, Kelley SS (2011) Ultrathin film coatings of aligned cellulose nanocrystals from a convective-shear assembly system and their surface mechanical properties. Soft Matter 7:1957–1967

Howarter JA, Youngblood JP (2008) Self-cleaning and next generation anti-fog surfaces and coatings. Macromol Rapid Commun 29:455–466

Hult EL, Iotti M, Lenes M (2010) Efficient approach to high barrier packaging using microfibrillar cellulose and shellac. Cellulose 17:575–586

Introzzi L, Fuentes-Alventosa JM, Cozzolino CA, Trabattoni S, Tavazzi S, Bianchi CL et al (2012) "Wetting Enhancer" pullulan coating for antifog packaging applications. ACS Appl Mater Interfaces 4:3692–3700

Isogai A, Saito T, Fukuzumi H (2011) TEMPO-oxidized cellulose nanofibers. Nanoscale 3:71–85

Jang W-S, Rawson I, Grunlan JC (2008) Layer-by-layer assembly of thin film oxygen barrier. Thin Solid Films 516:4819–4825

Kato Y, Kaminaga J, Matsuo R, Isogai A (2005) Oxygen permeability and biodegradability of polyuronic acids prepared from polysaccharides by TEMPO-mediated oxidation. J Polym Environ 13:261–266

Kontturi E, Johansson LS, Kontturi KS, Ahonen P, Thune PC, Laine J (2007) Cellulose nanocrystal submonolayers by spin coating. Langmuir 23:9674–9680

Krikorian V, Pochan DJ (2003) Poly (L-lactic acid)/layered silicate nanocomposite: fabrication, characterization, and properties. Chem Mater 15:4317–4324

Lange J, Wyser Y (2003) Recent innovations in barrier technologies for plastic packaging—a review. Packag Technol Sci 16:149–158

Lee DS, Yam KL, Piergiovanni L (2008) Chapter 4: Permeation of gas and vapor. In: Food packaging science and technology. CRC Press–Taylor & Francis Group, Boca Raton, London, New York, pp 58–59, 86–93

Li B, Logan BE (2004) Bacterial adhesion to glass and metal-oxide surfaces. Colloids Surf B 36:81–90

Li F, Biagioni P, Finazzi M, Tavazzi S, Piergiovanni L (2013) Tunable green oxygen barrier through layer-by-layer self-assembly of chitosan and cellulose nanocrystals. Carbohydr Polym 92:2128–2134

Lim LT, Auras R, Rubino M (2008) Processing technologies for poly(lactic acid). Prog Polym Sci 33:820–852

Lordan S, Kennedy JE, Higginbotham CL (2011) Cytotoxic effects induced by unmodified and organically modified

nanoclays in the human hepatic HepG2 cell line. J Appl Toxicol 31:27–35

Martinez-Sanz M, Lopez Rubio A, Lagaron JM (2012) On the optimization of the dispersion of unmodified bacterial cellulose nanowhiskers into polylactide via melt compounding to significantly enhance barrier and mechanical properties. Biomacromolecules 13:3887–3899

Mazeau K, Heux L (2003) Molecular dynamics simulations of bulk native crystalline and amorphous structures of cellulose. J Phys Chem B 107:2394–2403

Montaño-Leyva B, Ghizzi D, da Silva G, Gastaldi E, Torres-Chávez P, Gontard N, Angellier-Coussy H (2013) Biocomposites from wheat proteins and fibers: structure/mechanical properties relationships. Ind Crops Prod 43:545–555

Moon RJ, Martini A, Nairn J, Simonsen J, Youngblood J (2011) Cellulose nanomaterials review: structure, properties and nanocomposites. Chem Soc Rev 40:3941–3994

Muzzarelli RAA, Boudrant J, Meyer D, Manno N, DeMarchis M, Paoletti MG (2012) Current views on fungal chitin/chitosan, human chitinases, food preservation, glucans, pectins and inulin: a tribute to Henri Braconnot, precursor of the carbohydrate polymers science, on the chitin bicentennial. Carbohydr Polym 87:995–1012

No HK, Meyers SP, Prinyawiwatkul W, Xu Z (2007) Applications of chitosan for improvement of quality and shelf life of foods: a review. J Food Sci 72:R87–R100

Noorani S, Simonsen J, Atre S (2007) Nano-enabled microtechnology: polysulfone nanocomposites incorporating cellulose nanocrystals. Cellulose 14:577–584

Nuraje N, Asmatulu R, Cohen RE, Rubner MF (2010) Durable antifog films from layer-by-layer molecularly blended hydrophilic polysaccharides. Langmuir 27:782–791

Priolo MA, Gamboa D, Holder KM, Grunlan JC (2010) Super gas barrier of transparent polymer–clay multilayer ultrathin films. Nano Lett 10:4970–4974

Ray SS, Yamada K, Okamoto M, Ueda K (2002) Polylactide-layered silicate nanocomposite: a novel biodegradable material. Nano Lett 2:1093–1096

Ray SS, Yamada K, Okamoto M, Ueda K (2003) New polylactide-layered silicate nanocomposites. 2. Concurrent improvements of material properties, biodegradability and melt rheology. Polymer 44:857–866

Rhim J-W, Ng PKW (2007) Natural biopolymer-based nanocomposite films for packaging applications. Crit Rev Food Sci Nutr 47:411–433

Ringus DL, Moraru CI (2013) Pulsed Ligh inactivation of Listeria innocua on food packaging materials of different surface roughness and reflectivity. J Food Eng 114:331–337

Rodionova G, Saito T, Lenes M, Eriksen O, Gregersen O, Fukuzumi H et al (2012) Mechanical and oxygen barrier properties of films prepared from fibrillated dispersions of TEMPO-oxidized Norway spruce and Eucalyptus pulps. Cellulose 19:705–711

Sanchez-Garcia MD, Hilliou L, Lagaron JM (2010) Morphology and water barrier properties of nanobiocomposites of k/i-hybrid carrageenan and cellulose nanowhiskers. J Agric Food Chem 58:12847–12857

Sánchez-Valdes S, López-Quintanilla ML, Ramírez-Vargas E, Medellín-Rodríguez FJ, Gutierrez-Rodriguez JM (2006) Effect of ionomeric compatibilizer on clay dispersion in polyethylene/clay nanocomposites. Macromol Mater Eng 291:128–136

Shellenberger K, Logan BE (2001) Effect of molecular scale roughness of glass beads on colloidal and bacterial deposition. Environ Sci Technol 36:184–189

Siqueira G, Abdillahi H, Bras J, Dufresne A (2010) High reinforcing capability cellulose nanocrystals extracted from *Syngonanthus nitens* (Capim Dourado). Cellulose 17:289–298

Siró I, Plackett D (2010) Microfibrillated cellulose and new nanocomposite materials: a review. Cellulose 17:459–494

Svagan AJ, Åkesson A, Cárdenas M, Bulut S, Knudsen JC, Risbo J et al (2012) Transparent films based on PLA and montmorillonite with tunable oxygen barrier properties. Biomacromolecules 13:397–405

Tharanathan RN (2003) Biodegradable films and composite coatings: past, present and future. Trends Food Sci Technol 14:71–78

van Oss CJ (2003) Long-range and short-range mechanisms of hydrophobic attraction and hydrophilic repulsion in specific and aspecific interactions. J Mol Recognit 16:177–190

van Oss CJ (2006) In: Dekker M (ed) Interfacial forces in aqueous media. CRC Press, New York, pp 18–28, 93–107

Vert M, Schwarch G, Coudane J (1995) Present and future of PLA polymers. J Macromol Sci-Pure Appl Chem A32:787–796

Yang Y-H, Haile M, Park YT, Malek FA, Grunlan JC (2011) Super gas barrier of all-polymer multilayer thin films. Macromolecules 44:1450–1459

Yue Y, Zhou C, French A, Xia G, Han G, Wang Q et al (2012) Comparative properties of cellulose nano-crystals from native and mercerized cotton fibers. Cellulose 19:1173–1187

Zhang L, Sun J (2010) Layer-by-layer codeposition of polyelectrolyte complexes and free polyelectrolytes for the fabrication of polymeric coatings. Macromolecules 43:2413–2420

Zhou CJ, Wang QW, Wu QL (2012) UV-initiated crosslinking of electrospun poly(ethylene oxide) nanofibers with pentaerythritol triacrylate: effect of irradiation time and incorporated cellulose nanocrystals. Carbohydr Polym 87:1779–1786